Supplement of Hydrol. Earth Syst. Sci., 29, 5913–5930, 2025 https://doi.org/10.5194/hess-29-5913-2025-supplement © Author(s) 2025. CC BY 4.0 License.





Supplement of

Altitudinal variation in impacts of snow cover, reservoirs and precipitation seasonality on monthly runoff in Tibetan Plateau catchments

Nan Wu et al.

Correspondence to: Ke Zhang (kzhang@hhu.edu.cn)

The copyright of individual parts of the supplement might differ from the article licence.

The relative proportions of hydrological variables reflect their importance in hydrological processes, as shown in Figure S1. As both $\Delta S'$ and R exhibited negative values (Fig. 3), their absolute values were used in calculating the relative proportions, ensuring the relative proportions of P_r , S_{melt} , $\Delta S'$, R, and E summed up to 1. The proportion of P_r ($\frac{|P_r|}{|P_r| + |S_{melt}| + |\Delta S'| + |R| + |P_r|}$) increased from March to July, peaking at 50%, and decreased from August to November, with relative proportions in January, February, and December all below 6%. On the other hand, the relative proportion of $\Delta S'$ was higher from January to March and from November to February. S_{melt} primarily occurred in March and April, predominantly distributed in the GZ, ZB, DF, YJ, and ZS, with GZ having the highest proportion (44%). The relative proportions of R and E were generally greater than 10%, with the proportion of R being small from March to June, while E was prominent from February to May.

To clearly illustrate the long-term impacts of reduced snowmelt and reservoir construction on the seasonal dynamics of runoff at the outlet stations, Fig. S3 presents long-term time series (1980–2016) of total runoff, snowmelt runoff, and reservoir contributions. It can be observed that snowmelt and reservoirs contributed similarly to the annual runoff; however, reservoirs significantly altered the intra-annual runoff distribution pattern.

Figure Captions

40

Figure S1. Mean normalized monthly magnitude of the water balance term relative to the magnitude of all water balance terms, expressed as percentage from 0% (left part of grid cells, dark colors) to 100% (right, light).

Figure S2. Contribution box of different factors to R_v in 10 sub-basins, P_r , S_{melt} , $\Delta S'$ and E_0 represent rainfall, snowmelt, water storage change except snow, and potential evapotranspiration, respectively, P_r - $\Delta S'$, P_r - E_0 , S_{melt} - $\Delta S'$, S_{melt} - E_0 , and E_0 - $\Delta S'$ represent their covariance.

45 **Figure S3.** Time series of observed total runoff (i.e. monthly discharge volume divided by the total catchment area), runoff contribution of reservoir water storage change (calculated as monthly reservoir storage volume divided by total catchment area) and estimated snowmelt runoff (calculated as the monthly snowmelt volume divided by the total catchment area) from 1980 to 2017 for the whole basin.

Figure S4. Relationship between the monthly ratio of water demand to water supply $(E/(P_r + S_{melt} - \Delta S'))$ and monthly ratio of potential water demand to water supply $(E_0/(P_r + S_{melt} - \Delta S'))$ in the representative basin (LN, YJ and ZS).

Figure S5. Time series of estimated storage change (ΔS) and observed reservoir water storage change ($\Delta S_{Reservoirs}$) from 2002 to 2016 within the nested catchment of TZL.

Table Captions

55

Table S1. Parameter *n* values for 10 sub-basins and the annual average evapotranspiration calculated based on the Budyko and extended Budyko framework.

Table S2. The performance of extended Budyko framework in simulating evapotranspiration.

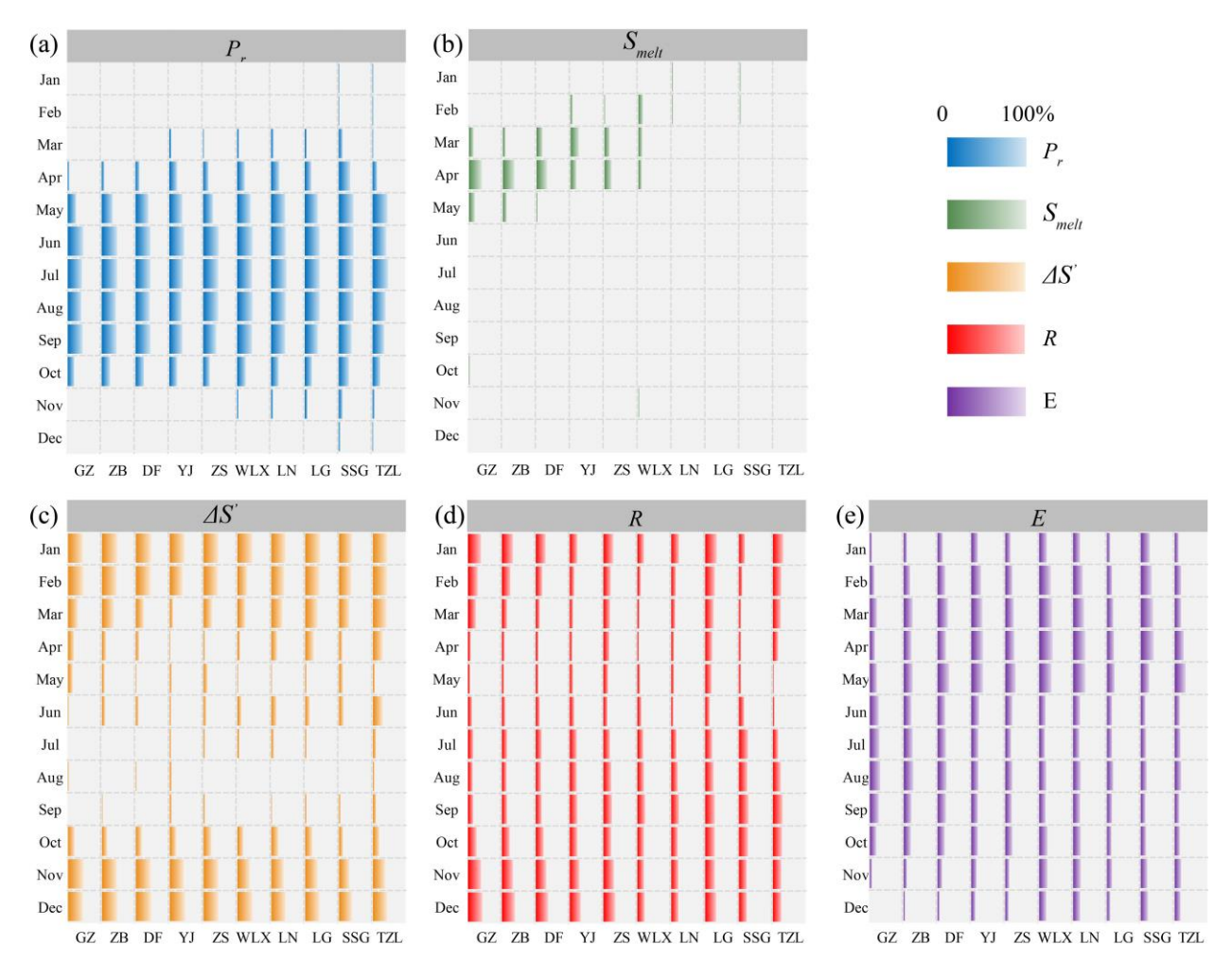


Figure S1. Mean normalized monthly magnitude of the water balance term relative to the magnitude of all water balance terms, expressed as percentage from 0% (left part of grid cells, dark colors) to 100% (right, light).

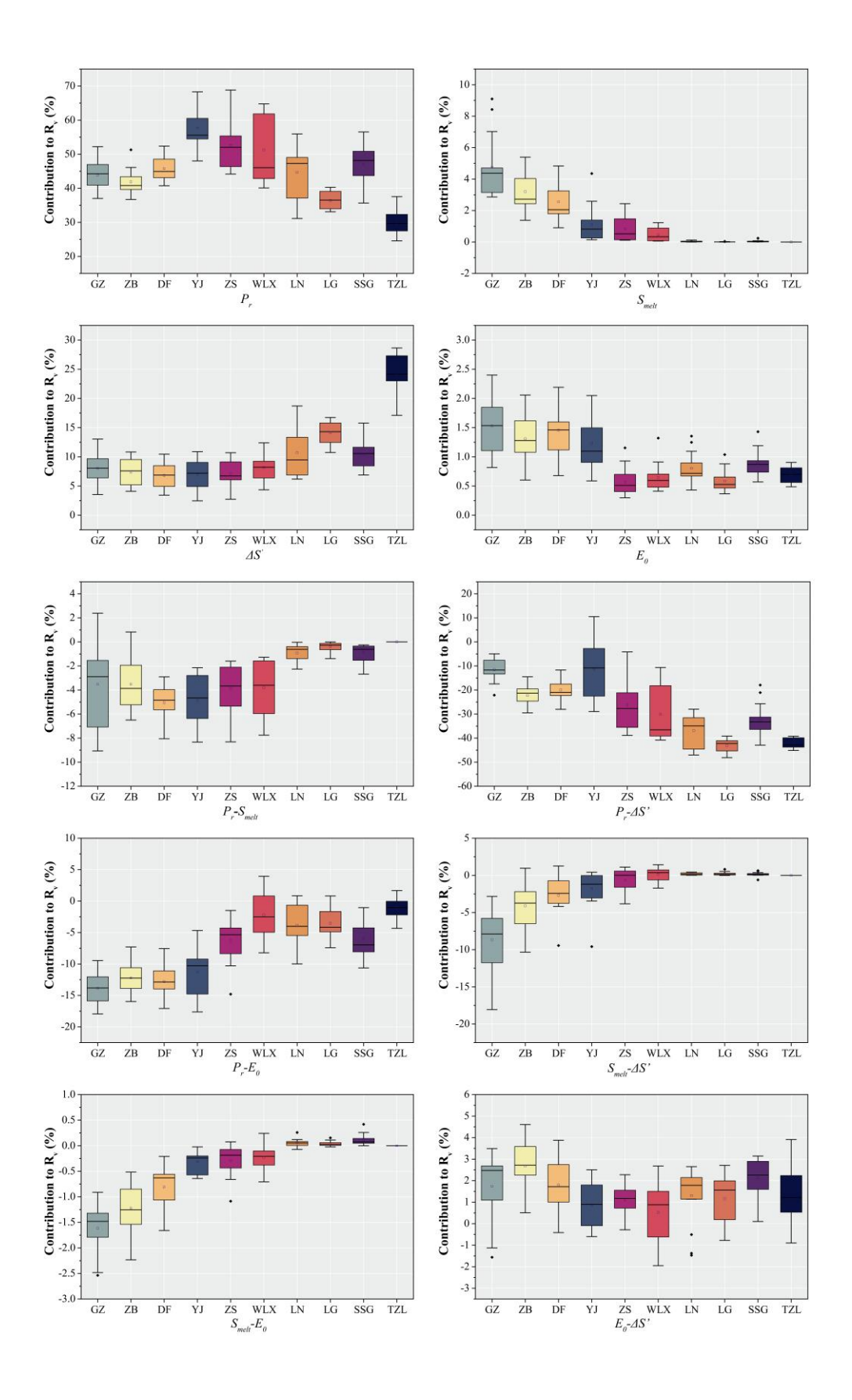


Figure S2. Contribution box of different factors to R_v in 10 sub-basins, P_r , S_{melt} , $\Delta S'$ and E_0 represent rainfall, snowmelt, water storage change except snow, and potential evapotranspiration, respectively. P_r - S_{melt} , P_r - $\Delta S'$, P_r - E_0 , S_{melt} - $\Delta S'$, S_{melt} - E_0 , and E_0 - $\Delta S'$ represent their covariance.

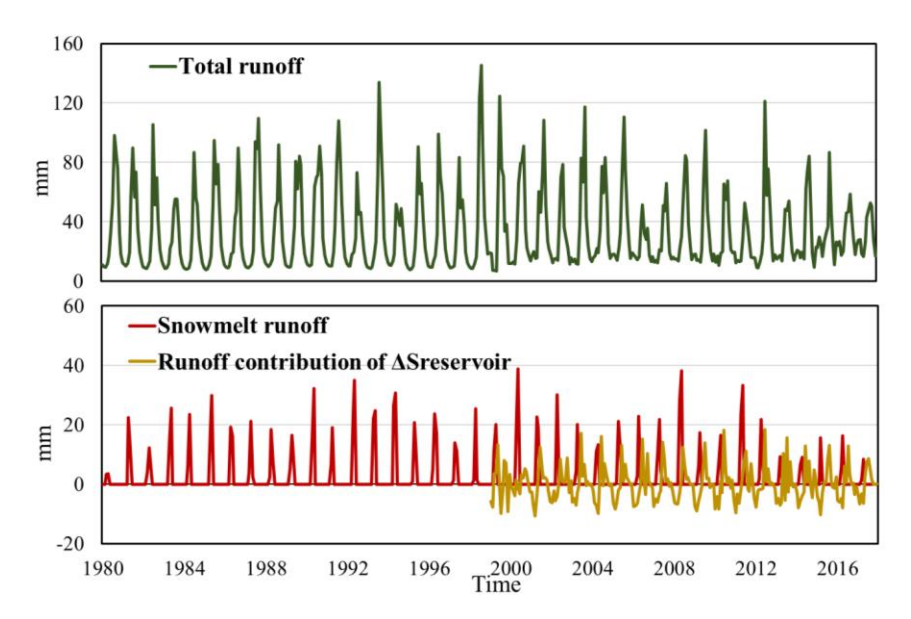


Figure S3. Time series of observed total runoff (i.e. monthly discharge volume divided by the total catchment area), runoff contribution of reservoir water storage change (calculated as monthly reservoir storage volume divided by total catchment area) and estimated snowmelt runoff (calculated as the monthly snowmelt volume divided by the total catchment area) from 1980 to 2017 for the whole basin.

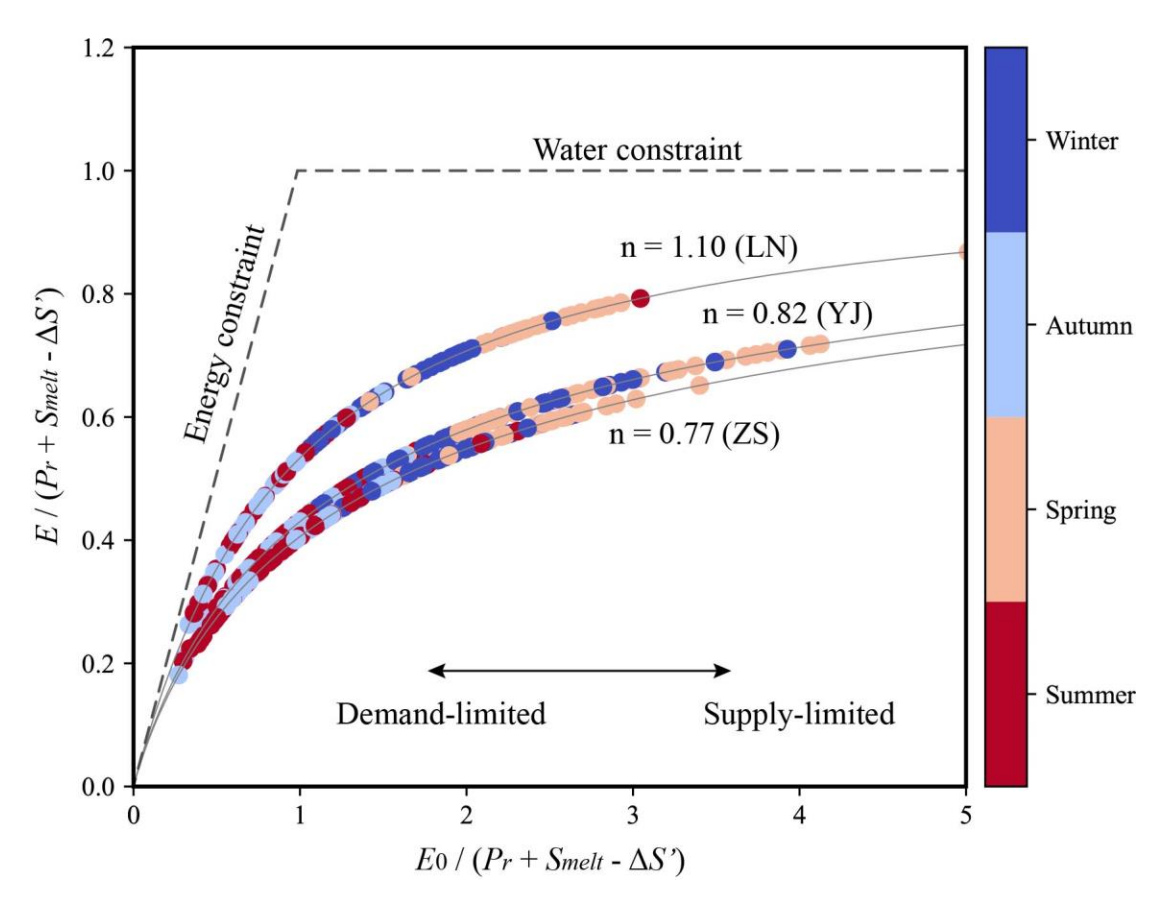


Figure S4. Relationship between the monthly ratio of water demand to water supply $(E/(P_r+S_{melt}-\Delta S'))$ and monthly ratio of potential water demand to water supply $(E_0/(P_r+S_{melt}-\Delta S'))$ in the representative basin (LN, YJ and ZS).

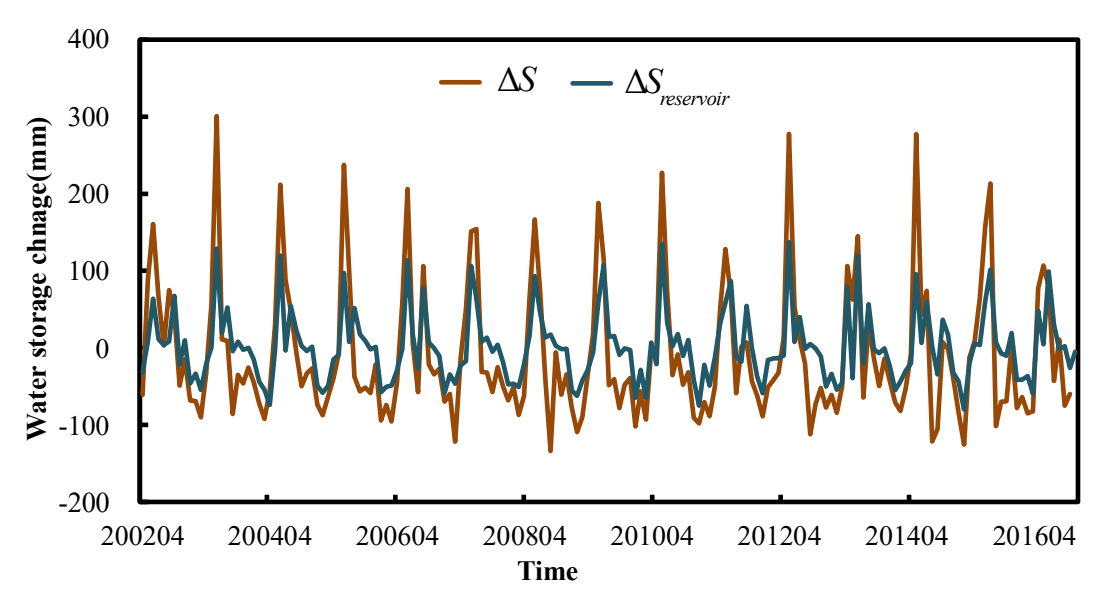


Figure S5. Time series of estimated storage change (ΔS) and observed reservoir water storage change ($\Delta S_{Reservoirs}$) from 2002 to 2016 within the nested catchment of TZL.

Table S1. Parameter n values for 10 sub-basins and the annual average evapotranspiration calculated based on the Budyko and extended Budyko framework.

Basin	GZ	ZB	DF	YJ	ZS	LN	WLX	LG	SSG	TZL
n	1.26	1.50	1.23	0.82	0.77	1.10	1.68	0.75	0.88	0.79
E_B (mm)	402	475	455	497	478	527	652	642	604	593
		479								

Table S2. The performance of extended Budyko framework in simulating evapotranspiration.

Basin	GZ	ZB	DF	YJ	ZS	LN	WLX	LG	SSG	TZL
NSE	0.87	0.81	0. 90	0.93	0.87	0.86	0.93	0.90	0.89	0.82